Diyala Journal of Engineering Sciences

Journal homepage: https://djes.info/index.php/djes

ISSN: 1999-8716 (Print); 2616-6909 (Online)

Kinetic Study of Ethanol Dehydration to Ethylene and Diethyl Ether in Catalytic Packed Bed Reactor Over ZSM-5 Catalyst

Narin A. Aali [1,*], Ghassan J. Hadi [2]

[1] Department of Chemical Engineering, Soran University, Erbil, Iraq
[2] Technical Institute, Northern Technical University, Adour, Iraq

ARTICLE INFO

Article history:
Received October 2, 2022
Revised April 4, 2023
Accepted April 6, 2023
Available online April 20, 2023

Keywords:
Dehydration
Kinetic models
Mathematical modeling
Ethanol

ABSTRACT

Dehydration of ethanol is one of the crucial processes as it is considered a green route for producing ethylene and diethyl ether and is promoted mainly by economics and environmental appeal. In this study, different kinetic models for ethanol dehydration to ethylene and diethyl ether were developed based on two parallel reactions and different mechanisms. Additionally, a mathematical model of a packed bed reactor was also suggested based on a set of hypotheses for investigating the axial concentration profile of ethanol. Kinetic parameters of each model were estimated by nonlinear regression analysis of obtained experimental data reported in the literature at temperatures between (523.15 – 623.15) K. The analysis showed that the single-site model I for ethylene formation and dual-site (LHHW) model for diethyl ether formation gave the best representation of experimental data compared to other proposed models. Kinetic parameters were found to be in good accordance with the Arrhenius equation with acceptable straight-line plots, and they have been satisfactorily correlated as functions of reaction temperature. The mathematical model presented a smooth linear change in ethanol concentration at various temperatures. The AARD% obtained for each chosen ethylene and diethyl ether formation model were about (1.4502-2.5978) and (0.9135-2.9394), respectively.

1. Introduction

Due to the trajectory of human civilization development in the last few centuries, fossil fuels have become one of the essential resources in the world to sustain the existence of human societies. However, this dependency on fossil fuels carries a risk with it as fossil fuels are not renewable but take millions of years to form under very peculiar conditions, and the source of such finite fuels is located in politically unstable regions. Furthermore, the continual use of these fossil fuels by chemical sectors and other industries has led to various environmental problems, including greenhouse gas emissions from exhaust gas. As the problems associated with fossil fuels became clear to the scientific community and researchers, renewable resources became a topic of interest. Due to its large-scale production, ethanol is an interesting candidate in the field of renewable chemicals for its valorization into ethylene, diethyl ether, and heavy hydrocarbons. It can also produce several oxygenated molecules, such as acetaldehyde and diethyl acetate [1]. Following the environmental legislation, ethanol dehydration has been boosted lately as a new and eco-friendly route. It also gained industrial importance due to its high yield and

* Corresponding author.
E-mail address: naa520h@cheme.soran.edu.iq
DOI: 10.24237/djes.2023.16203

sustainability compared to petrochemical processes.

Generally, ethanol dehydration forms ethylene as the main product, and significant amounts of diethyl ether are produced as the main co-product, while minor quantities of acetaldehyde and some hydrocarbons can be formed [2]. Several heterogeneous catalysts have been investigated for ethanol dehydration, including alumina, zeolites, and transition metal oxides [3]–[5]. Zeolites (e.g., ZSM-5) have attained the most attention among the researched catalysts due to their high selectivity and activity [6]. The Kinetics of heterogeneous catalytic reactions represents a delicate field due to the involvement of several factors. The catalyst belongs to a different phase with respect to reactants. Thus, besides the reaction step, adsorption and desorption steps should be added, increasing the modelling complexity.

The kinetics of chemical reactions can sometimes be expressed by power law expression through regressing experimental data. These kinetic expressions are applied to control industrial reactors and predict their performance over time because of their simplicity and ease of application. However, they have a restricted insight into the reaction mechanism and can be used only in a limited range of reaction conditions [7], [8]. Complex reaction mechanisms, like Langmuir-Hinshelwood-Hougen-Watson (LHHW) and Eley–Rideal (ER), that assume quasi equilibria of adsorption/desorption steps and specific rate controlling steps are also available for modeling and expressing kinetics of heterogeneous reactions [9]. Beccera et al. [10] developed a kinetic model for ethylene production from aqueous ethanol over ZSM-5 catalysts using the LHHW mechanism. Another LHHW model was proposed by Rossetti et al. [11] through regressing experimental data of Kagyrmanova et al. [12] that aimed to suggest a comprehensive simulation of ethanol to ethylene plant and connecting the microscopic to the ton scale of the overall process. Gayubo et al. [13] developed a kinetic model for converting aqueous bioethanol to hydrocarbons on a catalyst with a slow deactivation by coke that was prepared using a ZSM-5 zeolite catalyst treated with alkali for the purpose of generating mesopores zeolite structure and lessening its acidic strength. The proposed kinetic model estimated the distribution of product lumps, including C_1- C_3 paraffins, C_3-C_4olefins, ethylene, gasoline or C_5- C_{10}. For this reaction system, most published researches concern with modification of catalysts using different approaches [14]–[19] , the role of metal impregnation on the yield of products and catalyst activity [20]–[23], along with the comparison between activity and lifetime of different catalysts [24]. However, there are few works in the literature related to kinetics modeling and mathematical modeling of reactors for ethanol dehydration.

Kinetic modeling is used to identify critical reaction intermediates and rate controlling elementary reactions, providing vital information to design an improved catalyst. While mathematical modeling of reactors is usually used to solve issues of modernizing existing plants, developing alternative operational approaches, designing safety systems, enhancing the yield/conversion of desired products by minimizing the cost, and reducing the required number of full-scale experiments [25], [26].This existing gap in the literature is addressed in this investigation by proposing different kinetic models for ethylene and diethyl ether formation and suggesting a mathematical model for a packed bed reactor to study the axial concentration profile of ethanol.

2. Kinetic modeling

The reactions considered in the ethanol dehydration process were based on the work of Ghassan [27]. The experimental studies of his work were conducted in an isothermal fixed bed reactor, which applied ethanol in the vapor phase over four different catalysts under a total pressure of 1 atm. Two temperature ranges were considered according to the type of catalyst, (523.15-623.15) K for alumina and zeolites (ZSM-5 and 4A) and (363.15-393.15) K for resin, along with using W/F ratio of 0.38-1.166 (g_{cat}, hr⁄gmol). His results revealed that the main products on the surface of the catalysts were ethylene (C_2H_4) and diethyl ether $(C_2H_5)_2O$

according to the following parallel reaction scheme:

$$C_2H_5OH \rightleftarrows C_2H_4 + H_2O \quad (1)$$

$$2C_2H_5OH \rightleftarrows (C_2H_5)_2O + H_2O \quad (2)$$

Ghassan investigated the kinetic modeling of this reaction system on resin catalysts only, while kinetic modeling on other catalysts remains unstudied. This point is considered in the present work by developing several kinetic models based on different mechanisms. The following references are used for notation purposes:

$C_2H_5OH \longrightarrow$A; $C_2H_4 \longrightarrow$O; $H_2O \longrightarrow$W; $(C_2H_5)_2O \longrightarrow$ E

1⟶ Ethylene formation reaction;

2⟶ Diethyl ether formation reaction

2.1 Ethylene formation

For the ethylene formation reaction, three Langmuir-Hinshelwood-Hougen-Watson (LHHW) models are presented. This approach is mainly based on the Langmuir adsorption isotherm.

a. Single-site model I

The single-site model involves ethanol chemisorption on the active site of ZSM-5 catalyst, then surface reaction to form ethylene gas and adsorbed water, followed by water desorption [28]. The mechanism of this model is represented by the following steps:

Step 1: Ethanol chemisorption

$$A + S \underset{k_{-A1}}{\overset{k_{A1}}{\rightleftarrows}} A.S$$

Step 2: Surface reaction

$$A.S \underset{k_{-s1}}{\overset{k_{s1}}{\rightleftarrows}} W.S + O_{(g)}$$

Step 3: Water desorption

$$W.S \underset{k_{-DW1}}{\overset{k_{DW1}}{\rightleftarrows}} W + S$$

By assuming each step to be rate controlling, the following rate expressions were obtained as shown in Table 1.

Table 1: Single-site model I rate expressions

Rate controlling step	Rate expression	Equation Number
Ethanol chemisorption	$r_{AD1} = \frac{k_1\left(P_A - P_O P_W / K_{eq1}\right)}{\left(1 + P_O P_W \frac{K_{W1}}{K_{S1}} + P_{E1}K_{E1} + P_{W1}K_{W1} + P_I K_{I1}\right)}$	3
Surface reaction	$r_{S1} = \frac{k_1\left(P_A - P_O P_W / K_{eq1}\right)}{(1 + P_A K_{A1} + P_E K_{E1} + P_W K_{W1} + P_I K_{I1})}$	4
Water desorption	$r_{DW1} = \frac{k_1\left(P_A/P_O - P_W / K_{eq1}\right)}{(1 + P_A K_{A1} + P_A K_{A1} K_{S1}/P_O + P_E K_{E1} + P_I K_{I1})}$	5

b. Single-site model II

This model consists of the following steps: ethanol chemisorption on the ZSM-5 active site, then the surface reaction takes place to form adsorbed ethylene and water vapor, followed by the desorption step [28], as follows:

Step 1: Ethanol chemisorption

$$A + S \underset{k_{-A1}}{\overset{k_{A1}}{\rightleftarrows}} A.S$$

Step 2: Surface reaction

$$A.S \underset{k_{-s1}}{\overset{k_{s1}}{\rightleftarrows}} O.S + W_{(g)}$$

Step 3: Ethylene desorption

$$O.S \underset{k_{-DO1}}{\overset{k_{DO1}}{\rightleftharpoons}} O + S$$

Table 2 contains the rate expressions of each individual step as the rate controlling.

Table 2: Rate expressions of single-site model II

Rate controlling step	Rate expression	Equation number
Ethanol chemisorption	$r_{AD1} = \frac{k_1\left(P_A - P_O P_W / K_{eq1}\right)}{\left(1 + P_O P_W \frac{K_{O1}}{K_{S1}} + P_O K_{O1} + P_E K_{E1} + P_I K_{I1}\right)}$	6
Surface reaction	$r_{S1} = \frac{k_1\left(P_A - P_O P_W / K_{eq1}\right)}{(1 + P_A K_{A1} + P_E K_{E1} + P_O K_{O1} + P_I K_{I1})}$	7
Ethylene desorption	$r_{DO1} = \frac{k_1\left(P_A / P_W - P_O / K_{eq1}\right)}{(1 + P_A K_{A1} + K_{S1} K_{A1} P_A / P_W + P_E K_{E1} + P_I K_{I1})}$	8

c. Dual-site model

Based on the literature, it has been proposed that more than one active site can participate in ethanol dehydration reaction over ZSM-5 catalyst [29]. In the dual-site model, the chemisorbed ethanol reacts with an adjacent vacant site of the catalyst (S) to form adsorbed ethylene and water, then followed by the desorption of each product as represented below:

Step 1: Ethanol chemisorption

$$A + S \underset{k_{-A1}}{\overset{k_{A1}}{\rightleftharpoons}} A.S$$

Step 2: Surface reaction

$$A.S + S \underset{k_{-s1}}{\overset{k_{s1}}{\rightleftharpoons}} O.S + W.S$$

Step 3: Ethylene desorption

$$O.S \underset{k_{-DO1}}{\overset{k_{DO1}}{\rightleftharpoons}} O + S$$

Step 4: Water desorption

$$W.S \underset{k_{-DW1}}{\overset{k_{DW1}}{\rightleftharpoons}} W + S$$

The obtained rate expressions for this model are shown in Table 3.

Table 3: Rate expressions of dual-site model

Rate controlling step	Rate expression	Equation number
Ethanol chemisorption	$r_{AD1} = \frac{k_1\left(P_A - P_O P_W / K_{eq1}\right)}{\left(1 + P_O P_W \frac{K_{A1}}{K_{eq1}} + P_E K_{E1} + P_W K_{W1} + P_O K_{O1} + P_I K_{I1}\right)}$	9
Surface reaction	$r_{S1} = \frac{k_1\left(P_A - P_O P_W / K_{eq1}\right)}{(1 + P_A K_{A1} + P_E K_{E1} + P_W K_{W1} + P_O K_{O1} + P_I K_{I1})^2}$	10

Ethylene desorption
$$r_{DO1} = \frac{k_1\left(\frac{P_A K_{eq1}}{P_W} - P_O\right)}{\left(1 + P_A K_{A1} + P_W K_{W1} + \frac{P_A K_{eq1} K_{O1}}{P_W} + P_E K_{E1} + P_I K_{I1}\right)} \quad (11)$$

Water desorption
$$r_{DW1} = \frac{k_1\left(\frac{P_A K_{eq1}}{P_O} - P_W\right)}{\left(1 + P_A K_{A1} + \frac{P_A K_{eq1} K_{W1}}{P_O} + P_O K_{O1} + P_E K_{E1} + P_I K_{I1}\right)} \quad (12)$$

2.2 Diethyl ether formation

The kinetic models for diethyl ether formation were developed based on two different mechanisms, Langmiur-Hinshelwood-Hougen-Watson (LHHW) and Eley-Rideal. The details of each mechanism are given below.

a. LHHW model

According to this model, two adjacently chemisorbed ethanol molecules react to form chemisorbed diethyl ether and water as main products [29]. This model is represented by the following mechanism:

Step 1: Ethanol chemisorption

$$A + S \underset{k_{-A2}}{\overset{k_{A2}}{\rightleftarrows}} A.S$$

Step 2: Surface reaction

$$A.S + A.S \underset{k_{-S2}}{\overset{k_{S2}}{\rightleftarrows}} W.S + E.S$$

Step 3: Diethyl ether desorption

$$E.S \underset{-k_{DE2}}{\overset{k_{DE2}}{\rightleftarrows}} E + S$$

Step 4: Water desorption

$$W.S \underset{-k_{DW2}}{\overset{k_{DW2}}{\rightleftarrows}} W + S$$

Table 4 shows the rate expressions of each step as rate limiting one.

Table 4: Rate expressions of LHHW model for diethyl ether formation

Rate controlling step	Rate expression	Equation number
Ethanol chemisorption	$r_{AD2} = \frac{k_2\left(P_A - \sqrt{P_W P_E / K_{eq2}}\right)}{\left(1 + \sqrt{P_W P_E \frac{{K_{A2}}^2}{K_{eq2}}} + P_E K_{E2} + P_W K_{W2} + P_O K_{O2} + P_I K_{I2}\right)}$	13
Surface reaction	$r_{S2} = \frac{k_2 {K_{A2}}^2\left({P_A}^2 - P_W P_E / K_{eq2}\right)}{(1 + P_A K_{A2} + P_E K_{E2} + P_W K_{W2} + P_O K_{O2} + P_I K_{I2})^2}$	14
Diethyl ether desorption	$r_{DE2} = \frac{k_2\left({P_A}^2 - P_W P_E / K_{eq2}\right)}{\left(1 + P_A K_{A2} + P_W K_{W2} + \frac{{P_A}^2}{P_W}\frac{K_{E2}}{K_{eq2}} + P_O K_{O2} + P_I K_{I2}\right)}$	15
Water desorption	$r_{DW2} = \frac{k_2\left({P_A}^2 - P_W P_E / K_{eq2}\right)}{\left(1 + P_A K_{A2} + P_E K_{E2} + \frac{{P_A}^2}{P_E}\frac{K_{W2}}{K_{eq2}} + P_O K_{O2} + P_I K_{I2}\right)}$	16

b. Eley-Rideal model I

This model assumes that one ethanol molecule in the gas phase reacts directly with another chemisorbed ethanol molecule in the presence of a catalyst vacant site adjacent to forming chemisorbed diethyl ether and water as products [30]. The reaction sequence for this model is:

Step 1: Ethanol chemisorption

$$A + S \underset{k_{-A2}}{\overset{k_{A2}}{\rightleftharpoons}} A.S$$

Step 2: Surface reaction

$$A.S + A + S \underset{k_{-S2}}{\overset{k_{S2}}{\rightleftharpoons}} W.S + E.S$$

Step 3: Diethyl ether desorption

$$E.S \underset{-k_{DE2}}{\overset{k_{DE2}}{\rightleftharpoons}} E + S$$

Step 4: Water desorption

$$W.S \underset{-k_{DW2}}{\overset{k_{DW2}}{\rightleftharpoons}} W + S$$

The Eley-Rideal model I rate expressions are shown in Table 5.

Table 5: Rate expressions of Eley-Rideal model I

Rate controlling step	Rate expression	Equation number
Ethanol chemisorption	$r_{AD2} = \frac{k_2\left(P_A - P_W P_E / P_A K_{eq2}\right)}{\left(1 + K_{A2}P_W P_E / P_A K_{eq2} + P_E K_{E2} + P_W K_{W2} + P_O K_{O2} + P_I K_{I2}\right)}$	17
Surface reaction	$r_{S2} = \frac{k_2 K_{A2}\left(P_A{}^2 - P_W P_E / K_{eq2}\right)}{(1 + P_A K_{A2} + P_E K_{E2} + P_W K_{W2} + P_O K_{O2} + P_I K_{I2})^2}$	18
Diethyl ether desorption	$r_{DE2} = \frac{k_2\left(P_A{}^2 K_{eq2} / P_W - P_E\right)}{\left(1 + P_A K_{A2} + P_A{}^2 K_{E2} K_{eq2} / P_W + P_W K_{W2} + P_O K_{O2} + P_I K_{I2}\right)}$	19
Water desorption	$r_{DW2} = \frac{k_2\left(P_A{}^2 K_{eq2} / P_E - P_W\right)}{\left(1 + P_A K_{A2} + P_E K_{E2} + P_A{}^2 K_{W2} K_{eq2} / P_E + P_O K_{O2} + P_{I2} K_I\right)}$	20

c. Eley-Rideal model II

This model states that one ethanol molecule in the gas phase reacts with another chemisorbed ethanol molecule without requiring a catalyst vacant site, water goes directly into the gaseous phase while diethyl ether is chemisorbed [30], as shown below:

Step 1: Ethanol chemisorption

$$A + S \underset{k_{-A2}}{\overset{k_{A2}}{\rightleftharpoons}} A.S$$

Step 2: Surface reaction

$$A.S + A \underset{k_{-S2}}{\overset{k_{S2}}{\rightleftharpoons}} E.S + W_{(g)}$$

Step 3: Diethyl ether desorption

$$E.S \underset{-k_{DE2}}{\overset{k_{DE2}}{\rightleftharpoons}} E + S$$

Table 6 contains the rate expressions of all the steps involved in the Rideal-Eley II.

Table 6: Rate expressions of Eley-Rideal model II

Rate controlling step	Rate expression	Equation number
Ethanol chemisorption	$r_{AD2} = \frac{k_2\left(P_A - P_W P_E / P_A K_{eq2}\right)}{\left(1 + \frac{P_W P_E}{P_A}\frac{K_{E2}}{K_{S2}} + P_E K_{E2} + P_O K_{O2} + P_I K_{I2}\right)}$	21
Surface reaction	$r_{S2} = \frac{k_2 K_{A2}\left({P_A}^2 - P_W P_E / K_{eq2}\right)}{(1 + P_A K_{A2} + P_E K_{E2} + P_O K_{O2} + P_I K_{I2})}$	22
Diethyl ether desorption	$r_{DE2} = \frac{k_2 K_{E2}\left({P_A}^2 K_{eq2} / P_W - P_E\right)}{\left(1 + P_A K_{A2} + \frac{{P_A}^2}{P_W} K_{A2} K_{S2} + P_O K_{O2} + P_I K_{I2}\right)}$	23

d. Eley-Rideal model III

This model assumes that one ethanol molecule in the gas phase reacts with another chemisorbed ethanol molecule without requiring a catalyst vacant site as in (Rideal-Eley II), but in this model the water is chemisorbed while diethyl ether goes directly into the gaseous phase. The model is represented by the following steps:

Step 1: Ethanol chemisorption

$$A + S \underset{k_{-A2}}{\overset{k_{A2}}{\rightleftharpoons}} A.S$$

Step 2: Surface reaction

$$A.S + A \underset{k_{-S2}}{\overset{k_{S2}}{\rightleftharpoons}} W.S + E_{(g)}$$

Step 3: Water desorption

$$W.S \underset{-k_{DW2}}{\overset{k_{DW2}}{\rightleftharpoons}} W + S$$

The rate expressions of each step as rate controlling step are shown in Table 7 below.

Table 7: Rate expressions of Eley-Rideal model III

Rate controlling step	Rate expression	Equation number
Ethanol chemisorption	$r_{AD2} = \frac{k_2\left(P_A - P_W P_E / P_A K_{eq2}\right)}{\left(1 + \frac{P_W P_E}{P_A}\frac{K_{W2}}{K_{S2}} + P_W K_{W2} + P_O K_{O2} + P_I K_{I2}\right)}$	24
Surface reaction	$r_{S2} = \frac{k_2 K_{A2}\left({P_A}^2 - P_W P_E / K_{eq2}\right)}{(1 + P_A K_{A2} + P_W K_{W2} + P_O K_{O2} + P_I K_{I2})}$	25
Water desorption	$r_{DW2} = \frac{k_2 K_{W2}\left({P_A}^2 K_{eq2} / P_E - P_W\right)}{\left(1 + P_A K_{A2} + \frac{{P_A}^2}{P_E} K_{A2} K_{S2} + P_O K_{O2} + P_I K_{I2}\right)}$	26

3. Reactor modeling

This section describes the proposed mathematical model of a packed bed reactor that operates isothermally. The most relevant hypotheses used for the development of the model are: steady-state system, one-dimensional plug flow, pseudo-homogeneous, no radial dispersion effects, negligible change in the volumetric flow rate due to chemical reactions, constant physical properties of the fluid including density and velocity, along with negligible pressure drop throughout the system. Based on the restrictive assumptions presented above, the general mass balance can be written as follows:

$$u_s \frac{dC_i}{dz} + \rho_B R_i(C.T) = 0 \quad (27)$$

Boundary conditions: $C_i = C_{i0}$ at z = 0 (28)

This model is used to analyse the concentration profile of ethanol along the length of the reactor; a graphical representation of the proposed reactor is shown in Figure 1. A similar analysis was considered in the literature for modeling the catalytic reactors [31], [32].

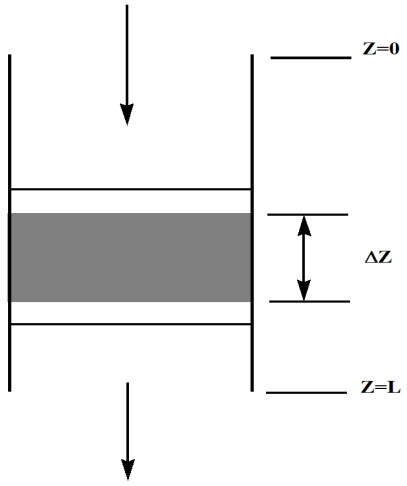

Figure 1. Graphical representation of the proposed packed bed reactor model

4. Result and discussion

4.1 Kinetic model analysis and parameter estimation

The experimental data required for solving the proposed kinetic models presented in sections 2.1 and 2.2 are derived from the experimental work of Ghassan [27]. These data include the partial pressure of each constituent, ethanol reaction rate, ethylene formation rate, and diethyl ether formation rate. Prior to solving these models, the thermodynamic equilibrium constant (K_{eq}) for temperatures 523.15, 548.15,573.15 and 623.15K for each reaction was estimated. Based on the reported values in the literature, the thermodynamic equilibrium constant (K_{eq}) of ethylene and diethyl ether at 363.15K are 1.89 and 43.81, respectively [27]. The Van 't Hoff equation is used for estimating values of (K_{eq}) at other mentioned temperatures as given below:

$$\ln \frac{K_{eq}(T)}{K_{eq}(T_1)} = \frac{\Delta H_R(T) - T\Delta Cp}{R}\left[\frac{1}{T_1} - \frac{1}{T}\right] + \frac{\Delta Cp}{R} \ln \frac{T}{T_1} \quad (29)$$

Values of ΔH_R for ethylene and diethyl ether formation were estimated to be (10728 cal/mol) and (-3032 cal/mol) respectively [33]. The Average heat capacity ΔCp was obtained for each temperature by using equation 30, the coefficients (A, B, C, D, and E) were taken from reference [34].

$$C_p = \text{A} + \text{BT} + \text{C}\,T^2 + \text{D}\,T^3 + \text{E}\,T^4 \quad (30)$$

Tables 8 shows the obtained values of (K_{eq}) for both ethylene and diethyl ether formation reactions, the temperature dependency of (K_{eq}) is also demonstrated in Figure 2.

Table 8: Equilibrium constant K_{eq} values of ethylene and diethyl ether formation reactions

Temperature (K)	ΔC_p(cal/mol K)		ΔH_R (cal/mol)		$K_{eq}(atm^{-1})$	
	ΔC_{p1}	ΔC_{p2}	ΔH_{R1}	ΔH_{R2}	K_{eq1}	K_{eq2}
523.15	3.3175	1.7015	10728	-3032	157.1964	11.3596
548.15	3.2255	1.6225			243.6445	9.79576
573.15	3.1417	1.5448			361.8130	8.54626
623.15	2.9989	1.3963			716.3467	6.70605

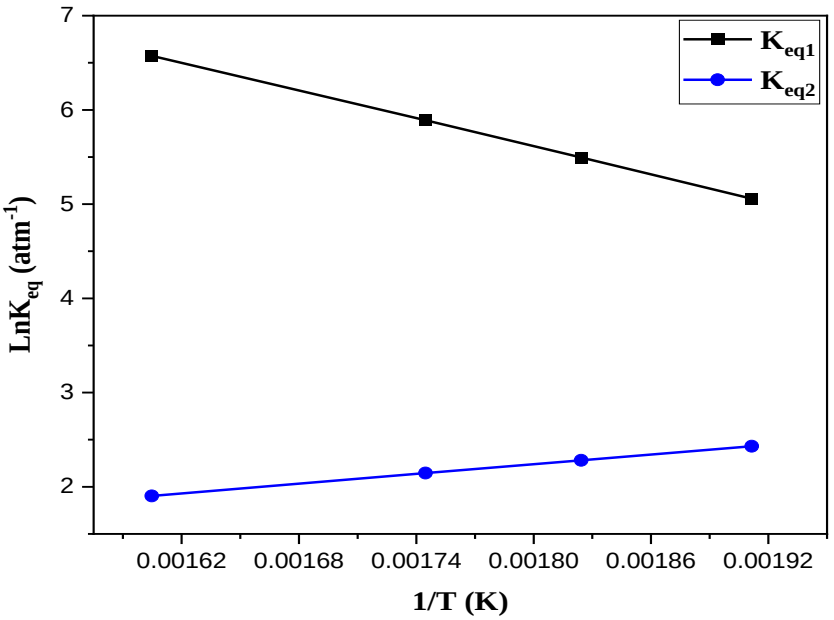

Figure 2. Variation of equilibrium constant K_{eq} with temperature

Nonlinear regression analysis in POLYMATH 6.10 software was used to find the best fit kinetic model with experimental data. Choosing the model was based on the minimum value of absolute average relative deviation AARD%, which is given by the following equation:

$$\text{AARD}= \sum \left|\frac{Y_{exp}-Y_{cal}}{Y_{exp}}\right| /N \times 100 \qquad (31)$$

When Y_{exp} is experimental reaction rate, Y_{cal} is the calculated reaction rate, and N is the number of data points. The regression results showed that the single-site model I with surface reaction-controlled step (equation 4) for ethylene and dual-site (LHHW) surface reaction-controlled model for diethyl ether formation (equation 14) gave the best representation of experimental data compared to other proposed kinetic models. The estimated values of kinetic parameters k_1 and k_2 along with adsorption equilibrium constants for both ethylene and diethyl ether at each temperature for both chosen models are shown in Table 9.

Table 9: The kinetic and adsorption equilibrium constant values of ethylene and diethyl ether formation reaction based on equations 4 and 14

Temperature (K)	523.15	548.15	573.15	623.15
$k_1\ (mol/g_{cat}.hr)$	0.00505	0.00736	0.00868	0.01370
$k_2\ (mol/g_{cat}.hr)$	0.00046	0.00124	0.00308	0.02791
$K_{A1}\ (atm^{-1})$	1.04002	1.08414	1.12604	1.20373
$K_{A2}\ (atm^{-1})$	0.07977	0.85796	7.50044	54.60495

The temperature dependence of these estimated parameters is also investigated as these parameters are a function of temperature. Figures 3 (a) and (b) show the variation of these parameters with temperature. It is clear that kinetic and adsorption equilibrium constant parameters follow the Arrhenius equation; according to that, the following expressions are obtained:

$$k_1 = 1.2842\ exp\left(\frac{-23.5220}{RT}\right) \quad (32)$$

$$k_2 = 1.2937 \times 10^6 exp\left(\frac{-94.6216}{RT}\right) \quad (33)$$

$$K_{A1} = 2.5862 exp\left(\frac{-3.9622}{RT}\right) \quad (34)$$

$$K_{A2} = 8.3243 \times 10^{14}\ exp\left(\frac{-157.2665}{RT}\right) \quad (35)$$

Under the same reaction conditions, the adsorption equilibrium constant of ethanol for the formation of diethyl ether is found to be relatively higher than that for the ethylene formation. This behaviour proposes that the dehydration of ethanol to form ethylene and diethyl ether occurs on different active sites of the ZSM-5 catalyst.

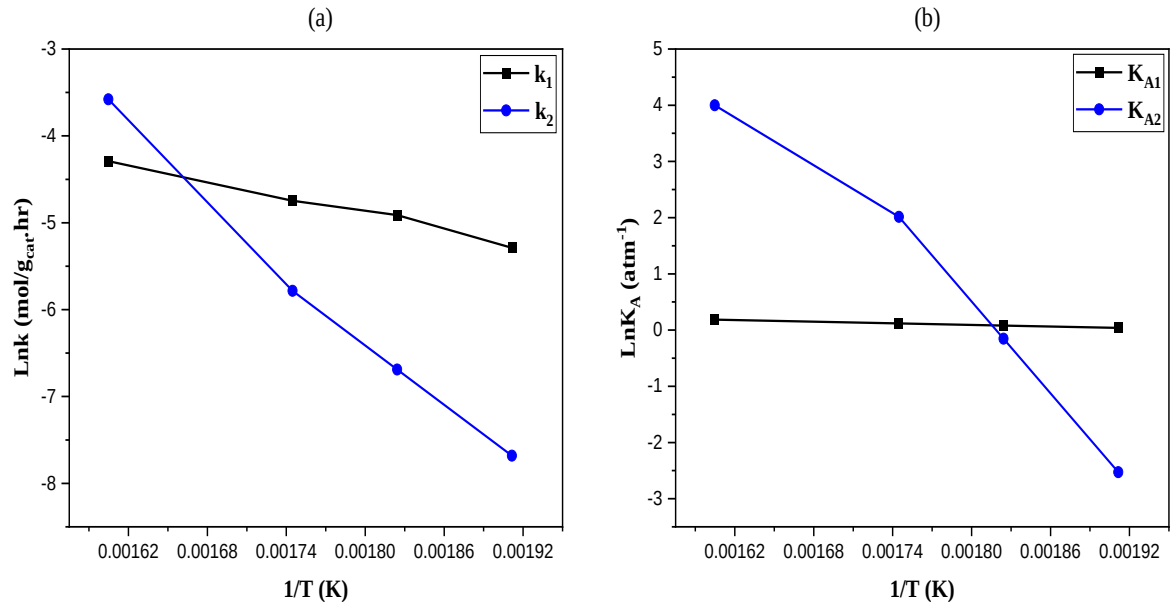

Figure 3. Variation of (a) kinetic and (b) adsorption equilibrium constant values of ethylene and diethyl ether formation reaction with temperature

The values of kinetic parameters are compared with values found in the literature, as shown in Table 10. There is an apparent difference between the estimated and literature values. This variation may result from using different temperature ranges, different experimental data, and differences in the applied method for estimating kinetic parameters.

Table 10: Comparison between literature and estimated values of k_1 and k_2

Temperature (K)	k_1 $(mol/g_{cat}.hr)$	k_2 $(mol/g_{cat}.hr)$	Reference
523.15	0.802	1.02	[31]
523.15	0.0738	-	[10]
548.15	0.0855	-	[10]
573.15	0.0864	-	[10]
623	0.000648	0.0009	[35]
488	0.000231	0.00576	[36]

Activation energies E_1 and E_2 along with pre-exponential factors A_1 and A_2 for both reactions were calculated by using Figure 3 (a), because they represent the linearized form of the Arrhenius equation as shown below:

$$\ln k_j = -\frac{E_j}{R}\left(\frac{1}{T}\right) + \ln A_j \quad (36)$$

The activation energy is obtained through a slope of the line and the pre-exponential factor is attained from the intercept. The estimated values of E_1 and E_2 are further compared with the literature, as demonstrated in Table 11.

Table 11: Comparison between calculated and literature values of activation energy

Activation energy		Reaction temperature (K)	Reference
Ethylene (kJ/mol)	Diethyl Ether (kJ/mol)		
23. 5220	94.6216	523.15-623.15	this study
189	159	503.15-623.15	[37]
14	-	553.15-573.15	[10]
33.8	-	623-723	[38]
133	80	673.15	[4]
39.5042	85.3333	500-800	[39]
193.530	47.210	483.15-543.15	[31]
57	-	424.15-633.15	[40]

One of the main factors that influence the activation energy is catalyst property. Regarding zeolite catalysts, the Si/Al ratio plays a vital role in changing the values of activation energy. It has been reported that high Si/Al ratios reduce the activation energy due to its higher interaction with reactant constituents [10]. Antonio et al. [4] estimated values of the pre-exponential factor for ethylene and diethyl ether formation as $(1.13 \times 10^6\ mol/g_{cat}.hr)$ and $(2.25 \times 10^3\ mol/g_{cat}.hr)$ respectively at temperatures lower than 673.15K, and Gayubo et al. [38] reported an A_1=283 $(mol/g_{cat}.hr)$. Other estimated parameters and AARD% for both models are listed in Table 12, no pertinent data were found in the literature to compare these estimated values with, due to the differences in the arrangement of the proposed rate expressions.

Table 12: Estimated model parameters of ethylene and diethyl ether formation using model presented in equations 4 and 14

Temperature (K)	523.15	548.15	573.15	623.15
K_{E1} (atm^{-1})	32.54745	35.23409	42.85514	57.8409
K_{W1} (atm^{-1})	4.846697	1.467458	4.483844	13.1094
K_{I1} (atm^{-1})	0.694172	0.576371	0.384379	0.57693
$(\text{AARD\%})_1$	1.660338	2.597770	1.450178	2.20786
K_{E2} (atm^{-1})	22.28196	17.36616	19.35379	83.7863
K_{W2} (atm^{-1})	2.064467	0.333399	61.30879	86.7665
K_{O2} (atm^{-1})	8.121068	5.09352	20.90733	89.1999
K_{I2} (atm^{-1})	0.607978	0.637303	1.954347	38.8528
$(\text{AARD\%})_2$	2.040975	0.913473	1.68023	2.939445

4.2 Comparison between the calculated and experimental reaction rates

Calculated and experimental values of reaction rate at a temperature range of (523.15-623.15) K are compared graphically in this section for ethylene formation through Figures 4a - 4d, and for diethyl ether formation through Figures 5a - 5d based on the proposed models in equation 4 and 14. According to the below results, there is a good agreement between calculated and experimental reaction rates, with a little deviation observed at some points related to the number of available data points as a small number of experimental data were available in the literature.

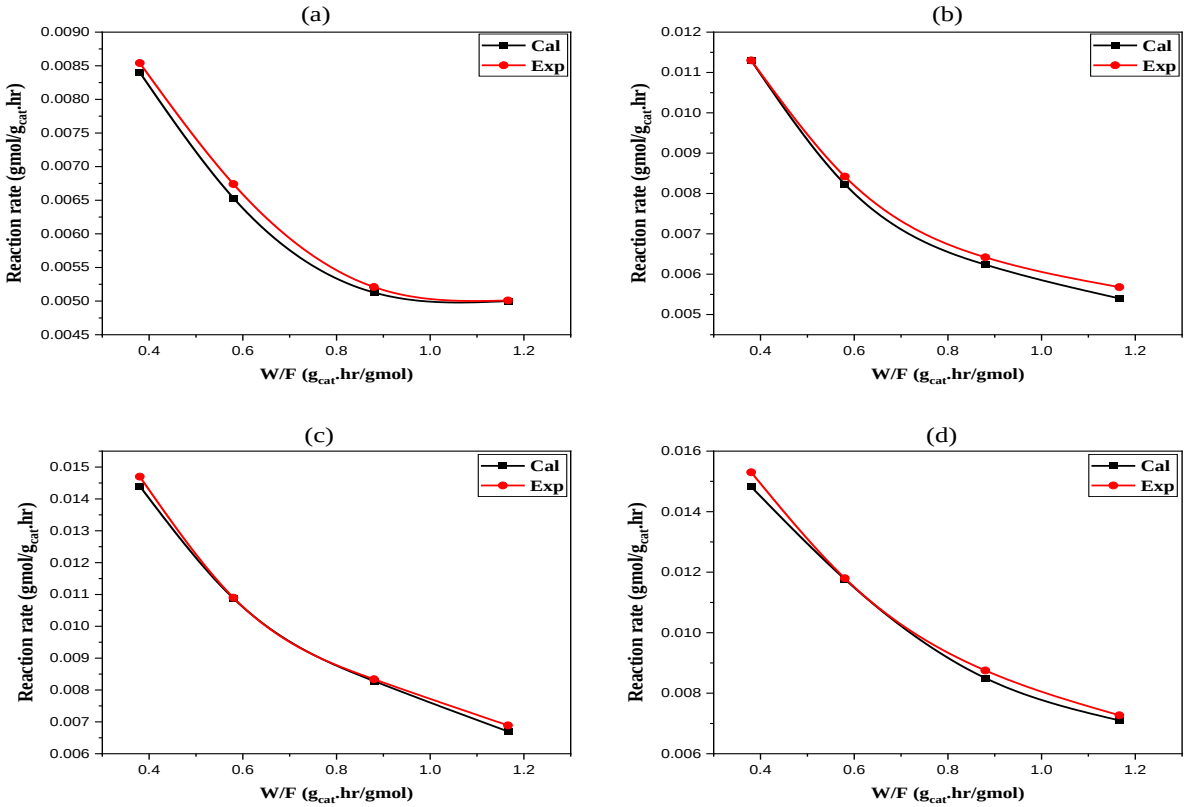

Figure 4. Comparison between the proposed model and the experimental results for ethylene formation reaction rate at (523.15-623.15) K from (a)-(d) respectively.

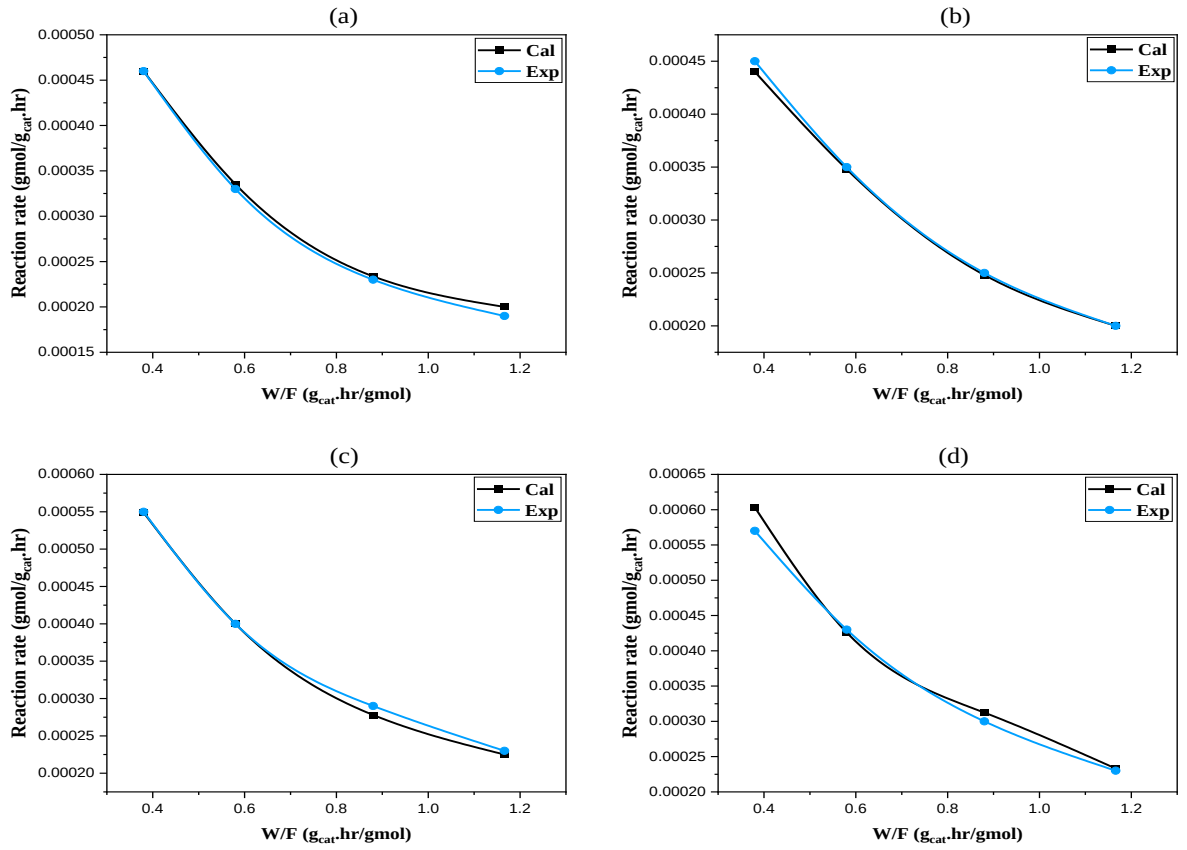

Figure 5. Comparison between the proposed model and the experimental results for diethyl ether formation reaction rate at (523.15-623.15) K from (a)-(d) respectively.

4.3 Further comparison with literature

The proposed kinetic models, equation 4 and 14 are further compared with another set of experimental data from reference[27]. The estimated model parameters and AARD% values for each model are listed in Table 13, and the comparison results are demonstrated graphically through Figures 6a-6d for ethylene formation and Figures 7a-7d for diethyl ether formation at temperature range of (523.15-623.15) K.

Table 13: Estimated model parameters of ethylene and diethyl ether formation using model presented in equations 4 and 14

Temperature (K)	523.15	548.15	573.15	623.15
$k_1(mol/g_{cat}.hr)$	0.0203	0.00434	0.00566	0.01068
$K_{A1}\ (atm^{-1})$	1.10735	1.15147	1.19338	1.27106
$K_{E1}\ (atm^{-1})$	7.3502	8.19044	20.51048	24.2706
$K_{W1}\ (atm^{-1})$	1.00209	4.26538	5.28295	7.07344
$K_{I1}\ (atm^{-1})$	0.07881	0.80899	0.64129	0.54956
$(\text{AARD\%})_1$	0.64012	2.69416	2.15456	1.53847
$k_2(mol/g_{cat}.hr)$	0.000761	0.00154	0.00337	0.08706
$K_{A2}\ (atm^{-1})$	0.56923	1.34741	12.547	60.125
$K_{E2}\ (atm^{-1})$	15.81099	25.3606	79.2991	98.1905
$K_{W2}\ (atm^{-1})$	3.86627	11.3965	31.62525	66.0791
$K_{O2}\ (atm^{-1})$	6.36828	9.01678	35.2430	99.9994
$K_{I2}\ (atm^{-1})$	0.75241	0.77035	0.42253	16.4007
$(\text{AARD\%})_2$	0	2.22664	1.36187	1.24248

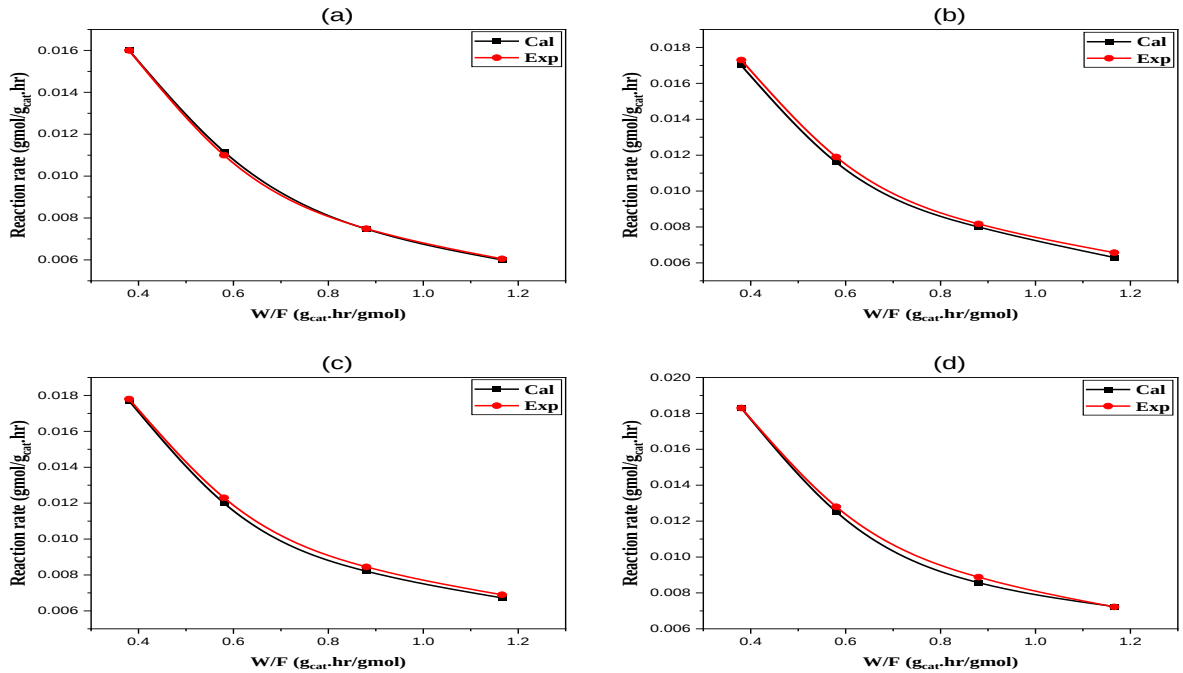

Figure 6. Comparison between the proposed model and the experimental results for ethylene formation reaction rate at (523.15-623.15) K from (a)-(d) respectively

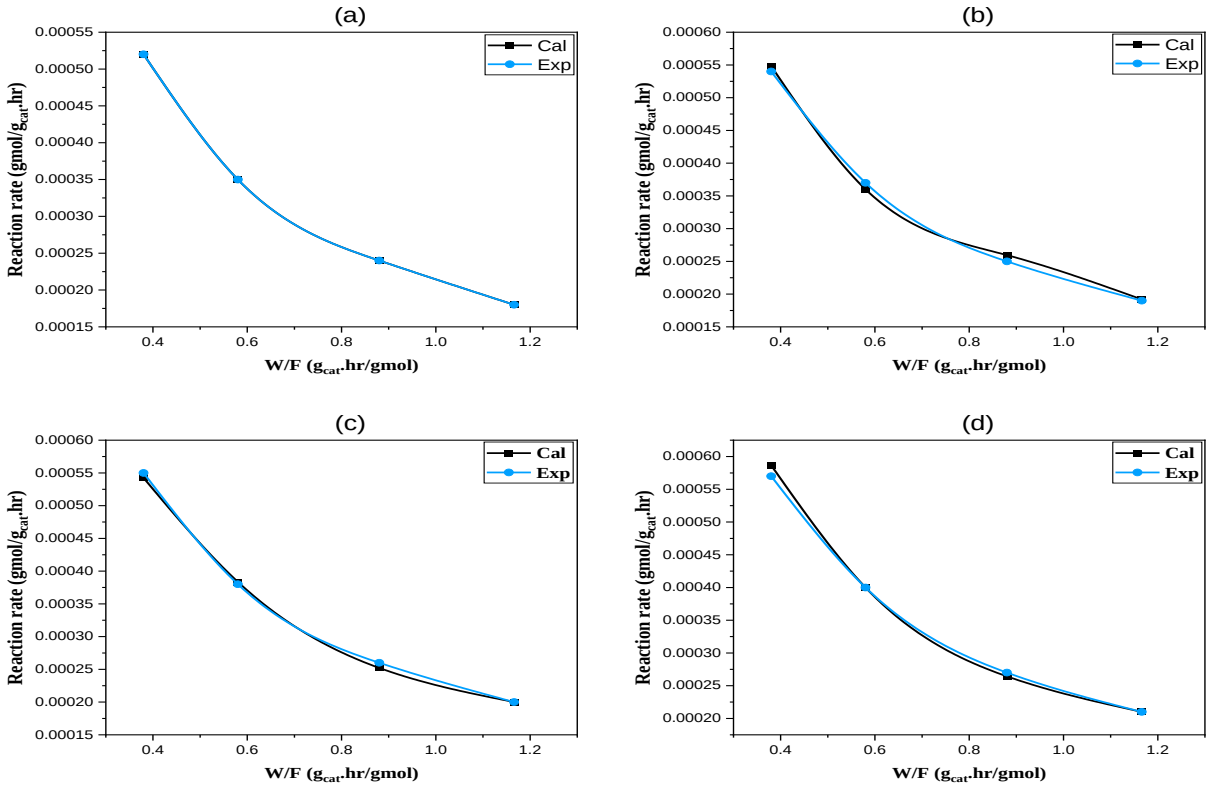

Figure 7. Comparison between the proposed model and the experimental results for diethyl ether formation reaction rate at (523.15-623.15) K from (a)-(d) respectively

According to the above results, the proposed models could successfully correlate the experimental data of both ethylene and diethyl ether formation rates with very small deviation.

4.4 Analysis of ethanol concentration profile

The concentration profile of ethanol along the length of the reactor was studied using the reactor design equation presented in section 3. A kinetic model is developed to represent the ethanol reaction rate ($-r_A$) as follows:

$$-r_A = \frac{k' P_A}{1+K_A' P_A} \quad (37)$$

The proposed kinetic model is based on the following assumptions:

a. Partial pressures of ethylene are smaller compared to the partial pressures of ethanol. Therefore, the contribution of ethylene to the adsorption term can be neglected.
b. The contribution of water is neglected because of its absence in the feed as pure ethanol was applied to the system.
c. Most polar components like ethanol and water are generally adsorbed substantially more than less polar components like diethyl ether because of the marked difference in dielectric constants. Thus, the contribution of diethyl ether can be neglected.
d. Negligible effect of the forward reaction term
e. Negligible effect of the inert on the rate of reaction.

The purpose behind using the above hypothesis is to reduce the complexity [41], [42]. Similar simplification analysis and kinetic models are also suggested in the literature [32], [35]. Required data for solving equation 37 was obtained from the work of Ghassan [27], and the rector data for the design equation was taken from the same reference, estimated values of the kinetic parameters are shown in Table 14.

Table 14: Estimated kinetic parameters of ethanol reaction rate based on equation 37

Temperature (K)	523.15	548.15	573.15	623.15
$k'\ (mol/g_{cat}.hr)$	0.1189643	0.1533384	0.3657129	0.5146619
$K_A'\ (atm^{-1})$	9.227561	9.013511	18.68639	27.21615

The reactor design equation is with respect to ethanol concentration, while the reaction rate equation $(-r_A)$ is according to the partial pressure of ethanol. To unify both expressions, the following equation of state is used:

$$P_i = C_i RT \quad (38)$$

By combining equations (27), (37), and (38) the final equation is obtained as follows:

$$u_s \frac{dC_A}{dz} = -\rho_B \frac{k' C_A RT}{1+K_A' C_A RT} \quad (39)$$

The above first-order differential equation was solved by using the numerical method Runge-Kutta 4thorder in MATLABE software under the boundary conditions stated in equation 28. The result showed a smooth linear change in the concentration of ethanol, as presented in Figure 8. This phenomenon can be related to the nature of the proposed model, applied hypothesis, the negligible effect of the backward reaction term, considering constant velocity along the reactor, and the presence of laminar flow inside the reactor. Similar results are also obtained in the literature for the dehydration process [32].

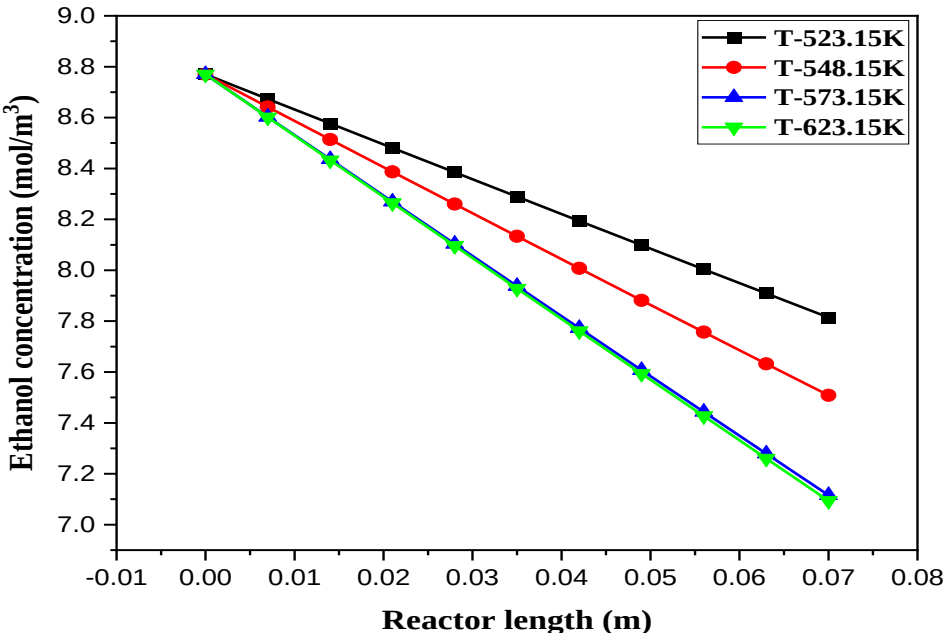

Figure 8. Axial concentration profile of ethanol predicted by equation 39

5. Conclusion

In this investigation, different kinetic models were proposed for the ethanol dehydration process to ethylene and diethyl ether formation by considering different reaction mechanisms. Using nonlinear regression analysis and the experimental data of reaction rate, the best-fit models were chosen for each constituent. According to the results, the single-sit model with surface reaction-controlled step for ethylene and LHHW dual-

site model with surface reaction step for diethyl ether formation gave the best representation of the experimental data compared with other proposed models. The models showed acceptable values of AARD% about (1.4502-2.5978) and (0.9135-2.9394), respectively, for ethylene and diethyl ether. The kinetic parameters of both models were determined and found to follow the Arrhenius equation at different temperatures. Activation energies for ethylene and diethyl ether formation were calculated to be 23.522 (kJ⁄mol) and 94.622 (kJ⁄mol), respectively. The estimated parameters were further compared with the literature. The observed variation between the parameters can be related to differences in proposed models by other researchers, applying different analysing techniques, working with different experimental data and reaction temperatures, along with using arrangement methods different from the one applied in this study. Based on a set of assumptions, a packed bed reactor model was proposed for examining the concentration gradient of ethanol through the reactor. The outcomes showed a straight change in the concentration profile that may result from the applied hypothesis and the presence of laminar flow in the real system from which the data was taken. It can be concluded from the proposed models that ethanol dehydration to form ethylene and diethyl ether are both surface reactions but require different active sites and proceed throughout different transition states.

References

[1] P. D. Srinivasan, K. Khivantsev, J. M. M. Tengco, H. Zhu, and J. J. Bravo-Suárez, "Enhanced ethanol dehydration on γ-Al_2O_3 supported cobalt catalyst," *J. Catal.*, vol. 373, pp. 276–296, 2019, doi: 10.1016/j.jcat.2019.03.024.

[2] R. Suerz *et al.*, "Application of microreactor technology to dehydration of bio-ethanol," *Chem. Eng. Sci.*, vol. 229, p. 116030, 2021, doi: 10.1016/j.ces.2020.116030.

[3] H. T. Abdulrazzaq, A. Rahmani Chokanlu, B. G. Frederick, and T. J. Schwartz, "Reaction Kinetics Analysis of Ethanol Dehydrogenation Catalyzed by MgO-SiO2," *ACS Catal.*, vol. 10, no. 11, pp. 6318–6331, 2020, doi: 10.1021/acscatal.0c00811.

[4] A. Tripodi, M. Belotti, and I. Rossetti, "Bioethylene production: From reaction kinetics to plant design," *ACS Sustain. Chem. Eng.*, vol. 7, no. 15, pp. 13333–13350, 2019, doi: 10.1021/acssuschemeng.9b02579.

[5] J. Lee, J. Szanyi, and J. H. Kwak, "Ethanol dehydration on γ-Al_2O_3: Effects of partial pressure and temperature," *Mol. Catal.*, vol. 434, pp. 39–48, 2017, doi: 10.1016/j.mcat.2016.12.013.

[6] K. Van Der Borght, V. V. Galvita, and G. B. Marin, "Ethanol to higher hydrocarbons over Ni, Ga, Fe-modified ZSM-5: Effect of metal content," *Appl. Catal. A Gen.*, vol. 492, pp. 117–126, 2015, doi: 10.1016/j.apcata.2014.12.020.

[7] A. H. Motagamwala and J. A. Dumesic, "Microkinetic Modeling: A Tool for Rational Catalyst Design," *Chem. Rev.*, vol. 121, no. 2, pp. 1049–1076, 2021, doi: 10.1021/acs.chemrev.0c00394.

[8] D. Y. Murzin, J. Wärnå, H. Haario, and T. Salmi, "Parameter estimation in kinetic models of complex heterogeneous catalytic reactions using Bayesian statistics," *React. Kinet. Mech. Catal.*, vol. 133, no. 1, pp.1-15, 2021, doi: 10.1007/s11144-021-01974-1.

[9] S. Matera, W. F. Schneider, A. Heyden, and A. Savara, "Progress in Accurate Chemical Kinetic Modeling, Simulations, and Parameter Estimation for Heterogeneous Catalysis," *ACS Catal.*, vol. 9, no. 8, pp. 6624–6647, 2019, doi: 10.1021/acscatal.9b01234.

[10] J. Becerra, E. Quiroga, E. Tello, M. Figueredo, and M. Cobo, "Kinetic modeling of polymer-grade ethylene production by diluted ethanol dehydration over H-ZSM-5 for industrial design," *J. Environ. Chem. Eng.*, vol. 6, no. 5, pp. 6165–6174, 2018, doi: 10.1016/j.jece.2018.09.035.

[11] I. Rossetti *et al.*, "Ethylene production via catalytic dehydration of diluted bioethanol: A step towards an integrated biorefinery," *Appl. Catal. B Environ.*, vol. 210, pp. 407–420, 2017, doi: 10.1016/j.apcatb.2017.04.007.

[12] A. P. Kagyrmanova, V. A. Chumachenko, V. N. Korotkikh, V. N. Kashkin, and A. S. Noskov, "Catalytic dehydration of bioethanol to ethylene: Pilot-scale studies and process simulation," *Chem. Eng. J.*, vol. 176–177, pp. 188–194, 2011, doi: 10.1016/j.cej.2011.06.049.

[13] A. G. Gayubo, A. Alonso, B. Valle, A. T. Aguayo, and J. Bilbao, "Kinetic model for the transformation of bioethanol into olefins over a HZSM-5 zeolite treated with alkali," *Ind. Eng. Chem. Res.*, vol. 49, no. 21, pp. 10836–10844, 2010, doi: 10.1021/ie100407d.

[14] M. Seifert *et al.*, "Ethanol to Aromatics on Modified H-ZSM-5 Part I: Interdependent Dealumination Actions," *ChemCatChem*, vol. 12, no. 24, pp. 6301–6310, 2020, doi: 10.1002/cctc.202001344.

[15] M. Seifert *et al.*, "Ethanol to Aromatics on Modified H-ZSM-5 Part II: An Unexpected Low Coking," *Chem. - An Asian J.*, vol. 15, no. 22, pp. 3878–3885, 2020, doi: 10.1002/asia.202000961.

[16] M. Limlamthong, N. Chitpong, and B. Jongsomjit, "Influence of phosphoric acid modification on catalytic properties of Al2O3 catalysts for dehydration of ethanol to diethyl ether," *Bull. Chem. React. Eng. & Catal.*, vol. 14, no. 1, pp. 1–8, 2019, doi: 10.9767/bcrec.14.1.2436.1-8.

[17] Z. Wu, J. Zhang, Z. Su, P. Wang, T. Tan, and F. S. Xiao, "Low-temperature dehydration of ethanol to ethylene over Cu- zeolite catalysts synthesized from cu-tetraethylenepentamine," *Ind. Eng. Chem. Res.*, vol. 59, no. 39, pp. 17300–17306, 2020, doi: 10.1021/acs.iecr.0c01253.

[18] A. Styskalik, V. Vykoukal, L. Fusaro, C. Aprile, and D. P. Debecker, "Mildly acidic aluminosilicate catalysts for stable performance in ethanol dehydration," *Appl. Catal. B Environ.*, vol. 271, no. April, p. 118926, 2020, doi: 10.1016/j.apcatb.2020.118926.

[19] L. Zeng, F. Liu, T. Zhao, and J. Cao, "Superior ZSM-5@γ-Al2O3Composite Catalyst for Methanol and Ethanol Coconversion to Light Olefins," *ACS Omega*, vol. 6, no. 29, pp. 19067–19075, 2021, doi: 10.1021/acsomega.1c02369.

[20] H. Mousavi, J. Towfighi Darian, and B. Mokhtarani, "Enhanced nitrogen adsorption capacity on Ca_2^+ ion-exchanged hierarchical X zeolite," *Sep. Purif. Technol.*, vol. 264, no. September 2020, p. 118442, 2021, doi: 10.1016/j.seppur.2021.118442.

[21] R. H. Gil-Horán, J. C. Chavarría-Hernández, P. Quintana-Owen, and A. Gutiérrez-Alejandre, "Ethanol Conversion to Short-Chain Olefins Over ZSM-5 Zeolite Catalysts Enhanced with P, Fe, and Ni," *Top. Catal.*, vol. 63, no. 5–6, pp. 414–427, 2020, doi: 10.1007/s11244-020-01229-8.

[22] M. C. H. Clemente, G. A. V. Martins, E. F. de Freitas, J. A. Dias, and S. C. L. Dias, "Ethylene production via catalytic ethanol dehydration by 12-tungstophosphoric acid@ceria-zirconia," *Fuel*, vol. 239, no. June 2018, pp. 491–501, 2019, doi: 10.1016/j.fuel.2018.11.026.

[23] T. K. Phung, L. P. Hernández, and G. Busca, "Conversion of Ethanol over transition metal oxide catalysts: Effect of tungsta addition on catalytic behaviour of titania and zirconia," *Appl. Catal. A Gen.*, vol. 489, pp. 180–187, 2015, doi: 10.1016/j.apcata.2014.10.025.

[24] K. K. Ramasamy and Y. Wang, "Catalyst activity comparison of alcohols over zeolites," *J. Energy Chem.*, vol. 22, no. 1, pp. 65–71, 2013, doi: 10.1016/S2095-4956(13)60008-X.

[25] C. G. Giovanni Chabot, Richard Guilet, Patrick Cognet, "A mathematical modeling of catalytic milli-fixed bed reactor for Fischer–Tropsch synthesis: Influence of tube diameter on Fischer Tropsch selectivity and thermal behavior," *J. Clean. Prod.*, vol. 87, no. 63–72, pp. 303–317, 2015.

[26] A. T. Jarullah, I. M. Mujtaba, and A. S. Wood, "Kinetic model development and simulation of simultaneous hydrodenitrogenation and hydrodemetallization of crude oil in trickle bed reactor," *Fuel*, vol. 90, no. 6, pp. 2165–2181, 2011, doi: 10.1016/j.fuel.2011.01.025.

[27] G. J. Hadi, "Kinetic Study of Catalytic Dehydration of Ethanol in Fixed Bed Catalytic Reactor," Ph.D dissertation, Al-Rasheed College of Eng. and Sc., Technology Univ., Baghdad, Apr. 2007.

[28] S. Shetsiri *et al.*, "Sustainable production of ethylene from bioethanol over hierarchical ZSM-5 nanosheets," *Sustain. Energy Fuels*, vol. 3, no. 1, pp. 115–126, 2019, doi: 10.1039/c8se00392k.

[29] K. Alexopoulos, M. John, K. Van Der Borght, V. Galvita, M. F. Reyniers, and G. B. Marin, "DFT-based microkinetic modeling of ethanol dehydration in H-ZSM-5," *J. Catal.*, vol. 339, pp. 173–185, 2016, doi: 10.1016/j.jcat.2016.04.020.

[30] R. Batchu *et al.*, "Ethanol dehydration pathways in H-ZSM-5: Insights from temporal analysis of products," *Catal. Today*, vol. 355, no. April, pp.

822–831, 2020, doi: 10.1016/j.cattod.2019.04.018.

[31] K. Y. Yoo, "Effects of reactor type on the economy of the ethanol dehydration process: Multitubular vs. adiabatic reactors," *Korean Chem. Eng. Res.*, vol. 59, no. 3, pp. 467–479, 2021, doi: 10.9713/kcer.2021.59.3.467.

[32] G. J. Hadi and A. J. Hadi, "Kinetic Study of Methanol Dehydration to Dimethyl Ether in Catalytic Packed Bed Reactor over Resin," *J. Mater. Sci. Chem. Eng.*, vol. 10, no. 06, pp. 45–58, 2022, doi: 10.4236/msce.2022.106005.

[33] K. van der Borght, K. Alexopoulos, K. Toch, J. W. Thybaut, G. B. Marin, and V. V. Galvita, "First-principles-based simulation of an industrial ethanol dehydration reactor," *Catalysts*, vol. 9, no. 11, pp. 1–21, 2019, doi: 10.3390/catal9110921.

[34] Carl L Yaws, "Chemical Properties Handbook*:Physical, Thermodynamics, Environmental Transport, Safety & Health Related Properties for Organic*." McGraw-Hill Education, 2000, pp. 34–52.

[35] M. Kang and A. Bhan, "Kinetics and mechanisms of alcohol dehydration pathways on alumina materials," *Catal. Sci. Technol.*, vol. 6, no. 17, pp. 6667–6678, 2016, doi: 10.1039/c6cy00990e.

[36] J. F. DeWilde, H. Chiang, D. A. Hickman, C. R. Ho, and A. Bhan, "Kinetics and mechanism of ethanol dehydration on γ-Al 2O3: The critical role of dimer inhibition," *ACS Catal.*, vol. 3, no. 4, pp. 798–807, 2013, doi: 10.1021/cs400051k.

[37] B. Laforce, "Upgrading of bioethanol : kinetic modeling of the catalytic conversion on zeolites" M.S. thesis, Faculty of Eng. and Archt., Ghent Univ., Belgium, 2013. [https://libstore.ugent.be/fulltxt/RUG01/002/033/374/RUG01-002033374_2013_0001_AC.pdf].

[38] A. G. Gayubo, A. T. Aguayo, A. M. Tarrio, M. Olazar, and J. Bilbao, "Kinetic modelling for deactivation by coke deposition of a HZSM-5 zeolite catalyst in the transformation of aqueous ethanol into hydrocarbons," *Stud. Surf. Sci. Catal.*, vol. 139, pp. 455–462, 2001, doi: 10.1016/s0167-2991(01)80230-5.

[39] R. B. Demuner, J. G. Soares Santos Maia, A. R. Secchi, P. A. Melo, R. W. Do Carmo, and G. S. Gusmao, "Modeling of Catalyst Deactivation in Bioethanol Dehydration Reactor," *Ind. Eng. Chem. Res.*, vol. 58, no. 8, pp. 2717–2726, 2019, doi: 10.1021/acs.iecr.8b05699.

[40] C. L. Chang, A. L. Devera, and D. J. Miller, "A lumped kinetic model for dehydration of ethanol to hydrocarbons over hzsm-5," *Chem. Eng. Commun.*, vol. 95, no. 1, pp. 27–39, 2010, doi: 10.1080/00986449008911464.

[41] B. V. R. Kuncharam and A. G. Dixon, "Multi-scale two-dimensional packed bed reactor model for industrial steam methane reforming," *Fuel Process. Technol.*, vol. 200, no. December 2019, p. 106314, 2020, doi: 10.1016/j.fuproc.2019.106314.

[42] A. G. Dixon and B. Partopour, "Computational Fluid Dynamics for Fixed Bed Reactor Design," *Annu. Rev. Chem. Biomol. Eng.*, vol. 11, no. 1, pp. 109–130, 2020, doi: 10.1146/annurev-chembioeng-092319-075328.

Nomenclature

S: Catalyst vacant site

P_i: Partial pressure of species *i* (atm).

K_{ij}: Adsorption equilibrium constant of species *i* in reaction *j* (atm^{-1})

k_j: Kinetic rate parameter for reaction *j* ($gmol/g_{cat}.hr$)

K_{eqj}: Thermodynamic equilibrium constant for reaction *j*. (units depend on reaction)

r_j: Reaction rate for reaction *j* ($gmol/g_{cat}.hr$)

u_s: Linear velocity of fluid (m/hr)

C_i: Concentration of species *i* (mol/m^3)

T: Temperature (K)

Z: Reactor axis coordinate (m)

L: Reactor length (m)

R: Gas constant ($J/mol.K$)

E_j: Activation energy for reaction *j* (kJ/mol)

A_j: Pre-exponential factor for reaction j $(mol/g_{cat}.hr)$

C_P: Heat capacity (cal/ mol K)

ΔC_P: Average heat capacity (cal/ mol K)

ΔH_R: Heat of reaction (cal/mol)

C_i°: initial concentration of species i (mol/m^3)

Greek letters

ρ_B: Bed density (kg/m^3)

Subscripts

i: Species

j: Reactions

eq: Equilibrium

1: Reaction 1

2: Reaction 2

Cat: catalyst

g: gram

A: Ethanol

O: Ethylene

W: Water I: Inert

E: Diethyl ether